Clays and Clay Minerals, Vol. 40, No. 1, 65–80, 1992.

SMECTITE-ILLITE TRANSITION IN BARBADOS ACCRETIONARY WEDGE SEDIMENTS: TEM AND AEM EVIDENCE FOR DISSOLUTION/CRYSTALLIZATION AT LOW TEMPERATURE

MARTINE D. BUATIER,[1] DONALD R. PEACOR, AND JAMES R. O'NEIL

Department of Geological Sciences, The University of Michigan, Ann Arbor, Michigan 48109

Abstract—Sediments from depths to 670 m in the Barbados accretionary complex and transecting the décollement zone have been studied by transmission and analytical electron microscopy (TEM/AEM). The sediments consist of claystone and mudstone intercalated with layers of volcanic ash. Smectite comprises the bulk of the noncalcareous sediments and forms a continuous matrix enveloping sparse, irregular, large grains of illite, chlorite, kaolinite and mixed-layer illite/chlorite of detrital origin at all depths. The detrital origin of illite is implied by illite-smectite textural relations, well-ordered 2*M* polytypism, and a muscovite-like composition. K is the dominant interlayer cation in smectite at all depths, in contrast to the Na and Ca that are normally present in similar rocks.

Deeper samples associated with the décollement zone contain small (up to 100 Å thick) illite packets included within still-dominant subparallel layers of contiguous smectite. AEM analyses of these packets imply illite-like compositions. Selected area electron diffraction (SAED) patterns show that this illite is the 1*M*d polytype. Packets display step-like terminations like those seen in illite of hydrothermal origin. The data collectively demonstrate that smectite transforms progressively to illite via a dissolution-recrystallization process within a depleting matrix of smectite, and not by a mechanism of layer replacement. This illite seems to form at depths as shallow as 500 m and temperatures of 20°–30°C, which is in marked contrast to the much higher temperature conditions normally assumed for this transformation. This implies that the high water/rock ratios associated with the décollement zone are significant in promoting reaction.

Key Words—Accretionary wedge, AEM analyses, Barbados, Electron diffraction, Fluid-sediment interaction, Illite, Mixed-layer, Smectite, TEM images.

INTRODUCTION

The smectite-to-illite transition is a fundamental process that occurs during diagenesis of argillaceous sediments, and yet most aspects of the transition are still controversial (e.g., Nadeau *et al.*, 1985; Yau *et al.*, 1987; Ahn and Peacor, 1986a, 1986b, 1989; Ransom and Helgeson, 1989; Inoue *et al.*, 1990). In addition, this reaction has been used as an empirical geothermometer because it has been commonly observed to occur at a given depth (temperature) (e.g., Hoffman and Hower, 1979). Others, however, have concluded that additional factors such as water/rock ratio affect the temperature of transformation (e.g., Freed and Peacor, 1989).

In the Barbados accretionary wedge, the tectonic structures that developed in front of the accreted zone favor fluid flow through permeable zones of the sediments. Anomalies in temperature and pore water geochemistry imply fluid migration pathways in the décollement zone (Blanc *et al.*, 1988; Fisher and Hounslow, 1990; Gieskes *et al.*, 1990). The influence of the sediments on the pore water chemistry is discussed in the Scientific Reports of the Ocean Drilling Program (Moore, Mascle *et al.*, 1990). Smectite dehydration was proposed to explain negative chloride anomalies in the pore water (Tribble, 1990). However, according to Capet *et al.* (1990) there is no evidence of clay diagenesis caused by thrusting or fluid migration in the sediments. On the other hand, X-ray powder diffraction (XRD) data for the clay fraction of the sediments demonstrated a decrease with depth in the proportion of the smectite component in mixed-layer illite/smectite (I/S), especially in the décollement zone and the underthrust sequence (Tribble, 1990). If such a transition occurs in the Barbados accretionary wedge, the presence of an ongoing transition in sediments where diagenesis is in progress offers a unique opportunity to define the mechanisms of clay mineral transitions. The data of Tribble (1990) imply that the transition can be detected in the sediments of the Barbados accretionary wedge at depths as shallow as 500 m, in proximity to the décollement zone. Because the low temperatures associated with such a shallow depth are at variance with application of a smectite/illite geothermometer, but consistent with enhanced water/rock ratio, characterization of the transition in those sediments would be of special significance.

Transmission and analytical electron microscopy (TEM and AEM) provide the means to make direct observations of submicron-sized clay minerals. Characterization of sequences representing the various stages

[1] Present address: Université des Sciences et Techniques de Lille, Laboratoire de dynamique sédimentaire et structurale, 596555 Villeneuve d'Ascq Cedex, France.

Copyright © 1992, The Clay Minerals Society

https://doi.org/10.1346/CCMN.1992.0400108 Published online by Cambridge University Press

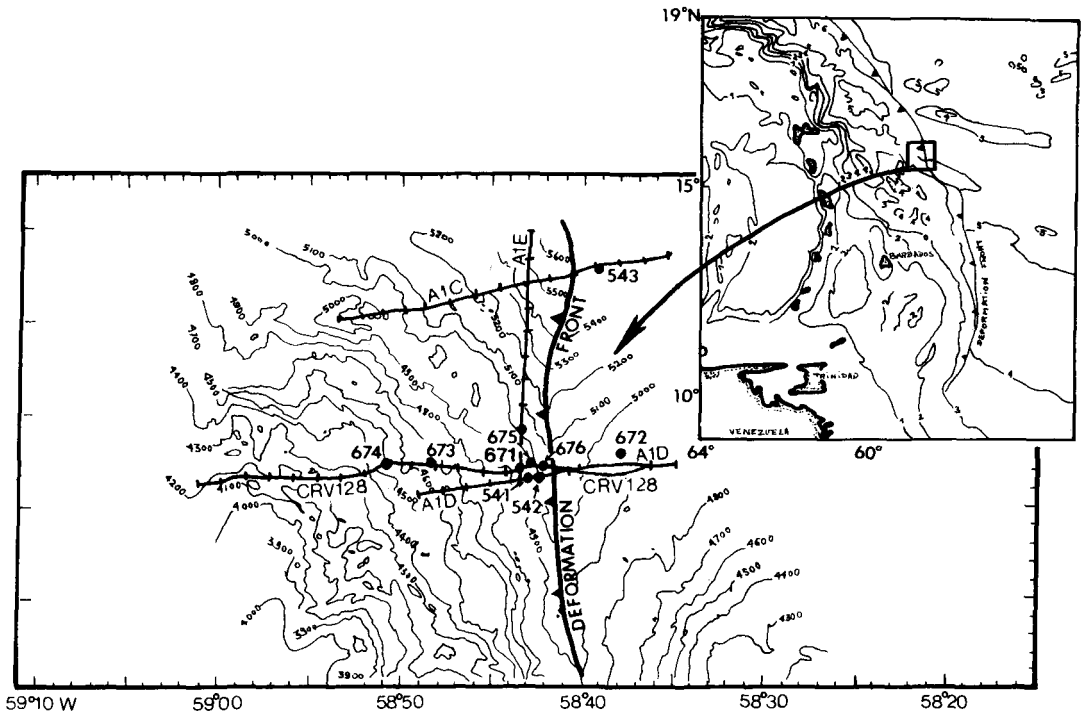


Figure 1. Location map of the drill site of Leg 110 in the Barbados accretionary complex (from Moore, Mascle *et al.*, 1990).

of transition can delineate transformation processes. This study was conducted utilizing those techniques to characterize the clay minerals and their evolution with depth, with emphasis on the mechanism of the smectite-to-illite transition.

GEOLOGICAL SETTING

The Barbados accretionary complex is located east of the Lesser Antilles island arc. The prism is about 300 km wide in the south but only 50 km in the north (Figures 1, 2). This change in width reflects the decreasing rate of growth of the complex. As a consequence of subduction, the Lesser Antilles volcanic arc developed during the Paleocene (Leclerc-Vanhoeve and Stephan, 1985) and the Neogene section are accreting at the deformation front with a 40% shortening within 7 km. Heat flow calculations suggest that fluid flow occurs with a periodicity on the order of tens of thousands of years (Fisher and Hounslow, 1990).

The lithology of samples from hole 671B, located in the deformation front, is described in Figure 3. The sequence is similar to that observed at site 672 located in the abyssal plain, except that underthrusting of the sediments created an abnormal contact at 130 meters below the sediment-sea water interface between late Pleistocene and early Pleistocene sections. Pliocene and Pleistocene sediments are calcareous. The lower Oligocene and Eocene sequences consist of alternating

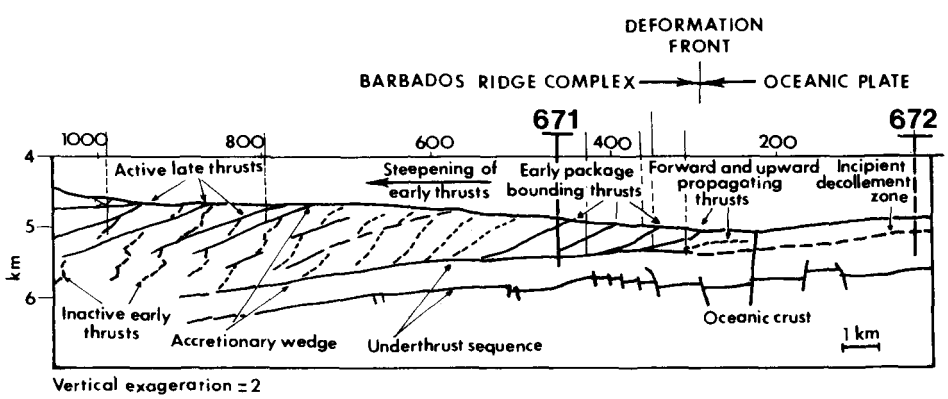


Figure 2. Cross section of the northern Barbados accretionary prism. Important structural features and the positions of sites 671 and 672 are represented (from Moore, Mascle *et al.*, 1990).

https://doi.org/10.1346/CCMN.1992.0400108 Published online by Cambridge University Press

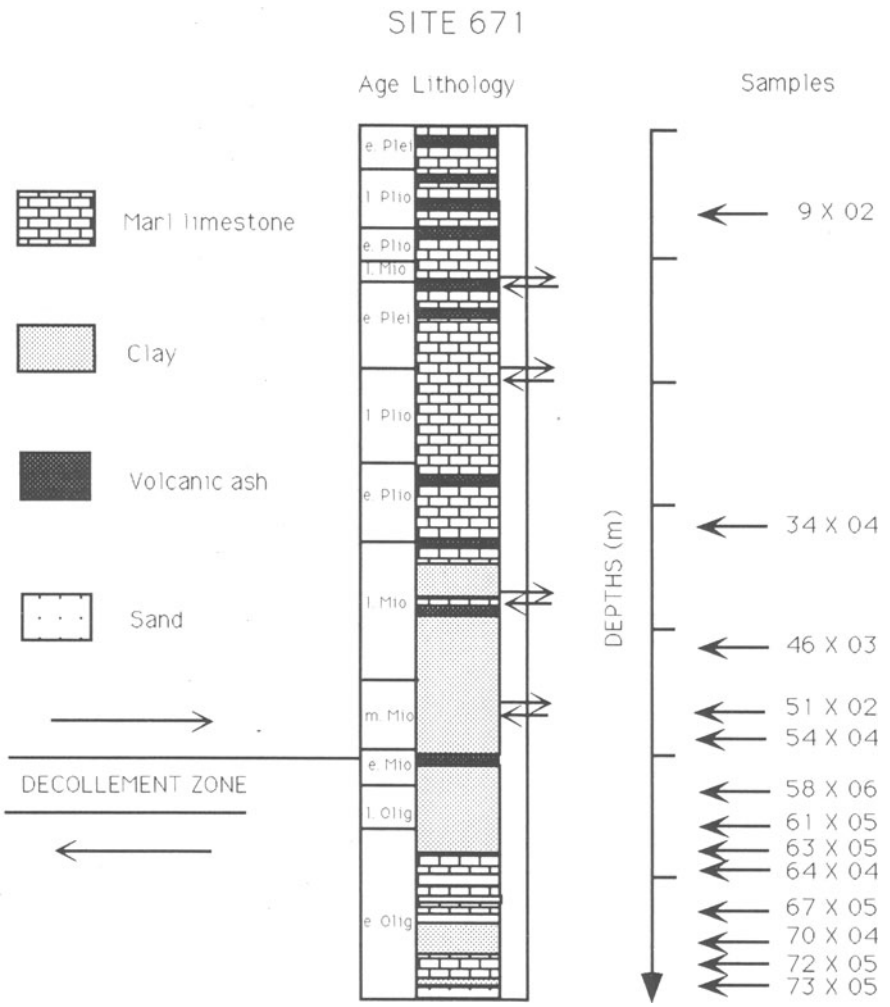


Figure 3. Summary of stratigraphic relations for site 671B Leg 110, with sample locations.

calcite-rich and calcite-free sediments, the latter being clay-rich. The Miocene sequences are essentially clay-rich sediments. Furthermore, the thickness of the late Miocene and middle Miocene section has increased as a result of the thrusting. According to previous XRD analyses, smectite is the dominant clay mineral in sediments of the Barbados accretionary wedge (Capet *et al.*, 1990; Tribble, 1990). Capet *et al.* (1990) noted the presence of quartz, plagioclase, calcite, and some other minor accessory minerals such as amphibole, gibbsite, and clinoptilolite. They observed an increase in the proportion of smectite with depth that correlated with an increase in the total clay content. Oligocene strata are underconsolidated at site 671; indeed the sediments are more porous than at site 672 (Taylor and Leonard, 1990). This underconsolidation increases with depth below the seafloor.

Examination of the physical properties and the clay minerals indicates that mineralogical changes occur in sediments being underthrusted (Moore, Mascle *et al.*, 1990). Geochemical signatures of pore fluids reflect a significant flux of fluids through the accretionary prism, with chemical anomalies along the décollement zone (anomalies in methane and chloride concentrations; Gieskes *et al.*, 1990). The occurrence and distribution of methane suggest that decomposition of organic carbon-rich sediments occurs in the deepest part of the prism. The low chloride concentration has been postulated to result from dehydration concomitant with the smectite-to-illite transition that occurs at higher temperatures and overburden pressures at depth (Tribble, 1990). Using XRD peak areas, Tribble (1990) obtained semiquantitative values for the proportions of clay minerals and estimated that the clay fraction contained 10 to 90% smectite (average of 52%), 0 to 36% illite (average of 18%) and 7 to 70% kaolinite + chlorite (average of 30%). Furthermore, she reported the presence of less than 20 ± 10% illite component in illite-

https://doi.org/10.1346/CCMN.1992.0400108 Published online by Cambridge University Press

smectite mixed layers from above the décollement zone at a depth of 500 m, increasing to more than 40 ± 20% in samples below the décollement zone. These data reflect the presence of a smectite-to-illite transition in the sediments of the Barbados accretionary wedge.

MATERIALS AND METHODS

The samples analyzed in this study are from drill hole 671, ODP Leg 110 (Figures 1, 2). Samples from this site were chosen because of its location in the accreted sediments and because it cuts across the décollement zone. XRD data were obtained on 13 samples located at different depths in the sedimentary column (Figure 3). Transmission and analytical electron microscope observations were made on a selection of seven samples, located both above and below the décollement zone, at depths of 65 meters (671B 9-2 [129–131], lower Pliocene), 300 meters (671B 34-3 [127–130] early Pliocene), 415 meters (671B 46-3 [127–130] late Miocene), 460 meters (671B 51-2 [102–104] middle Miocene), 600 meters (671B 64-4 [106–109] early Miocene), and 665 meters (671B 72X [38–40] early Oligocene) below the sea water-sediment interface (Figure 3). The samples consist both of carbonate- and clay-rich sediments.

In preparation for XRD analysis, each sample was dried in air, dispersed in deionized water, and then ultrasonically disaggregated before separation of the <2-μm fraction by settling in a water column. That fraction was pipetted onto glass slides and allowed to dry in air. The analyses were performed with a Philips X-ray diffractometer utilizing a scintillation detector, graphite monochromator, CuKα radiation, and theta-compensating slits. The diffractometer was controlled by a Databox system and microcomputer.

Samples retaining their original textures were embedded under vacuum in a Castolite epoxy resin, from which "sticky wax" thin sections were prepared. They were examined using scanning electron microscopy (SEM), including backscattered electron (BSE) imaging and energy dispersive spectroscopic (EDS) analyses to obtain general mineralogical and textural data in preparation for selection of areas appropriate for TEM analysis. Selected areas of the thin sections were removed and ion milled for TEM examination and chemical analysis using a Philips CM12-STEM fitted with a Kevex Quantum detector and analyzing system. Crystal shapes, especially (001) cross sections, were obtained from samples prepared by dispersion of clay particles on holey carbon-coated Cu grids.

The STEM was operated at 120 kV. Lattice-fringe images were obtained using only 001 reflections with a 10-μm diameter objective aperture that included 00l reflections with $l \leq 2$. Images were realized for three focus conditions, 0, +1000 Å, and −1000 Å. Chemical analyses were obtained in STEM mode only for areas that were first characterized by TEM and lattice-fringe

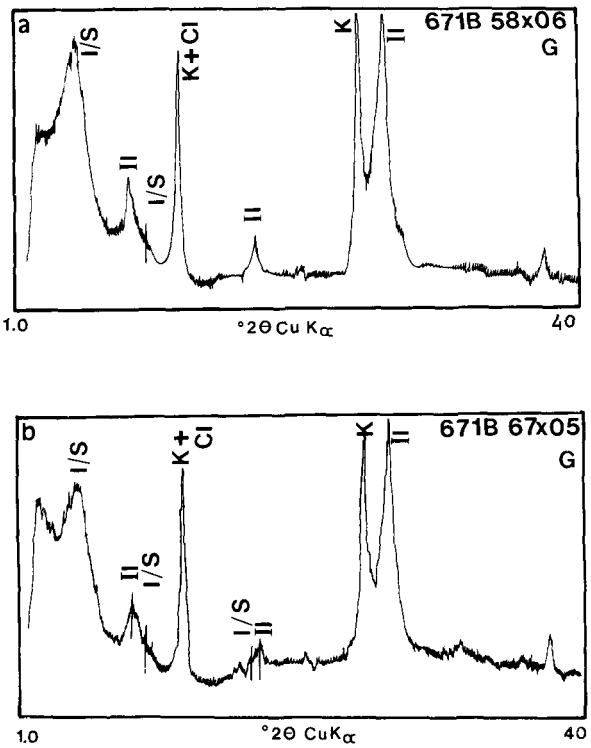


Figure 4. X-ray diffraction patterns of two glycolated samples (<2-μm fraction). (a) Sample located at 520 meters with smectite (<20% mixed-layer illite) and detrital clay minerals. (b) Deeper sample located below the décollement zone (620 meters) with mixed-layer illite/smectite (40–50% illite layers), and detrital clay minerals. I/S = random mixed-layer I/S; IL = detrital illite; K + Cl = kaolinite and chlorite.

imaging. Analyses were carried out using a square raster 1000 Å-wide to minimize diffusion of alkali ions. Quantitative analyses were obtained following the procedures of Cliff and Lorimer (1975) and Lorimer and Cliff (1976). Standard minerals that were used to obtain proportionality constants (k values) for each element relative to Si included muscovite for Al and K, albite for Na, sphene for Ca and Ti, and chlorite for Mg and Fe.

RESULTS

X-ray powder diffraction data

The aim of the XRD study was to characterize the mineralogy of the specific samples studied by TEM and not to repeat the detailed studies made by Capet *et al.* (1990) and Tribble (1990). XRD data described in this study were obtained only on the <2-μm fraction of the sediments. An intense and very sharp 15.5–16 Å peak due to (001) of mixed-layer illite-smectite (I/S) was observed for all specimens. This peak shifted to 17.2 Å after glycerol treatment (Figure 4). The same peak is less intense for sample 671B 9-2 (129–131), but only because of the high calcite content of this

https://doi.org/10.1346/CCMN.1992.0400108 Published online by Cambridge University Press

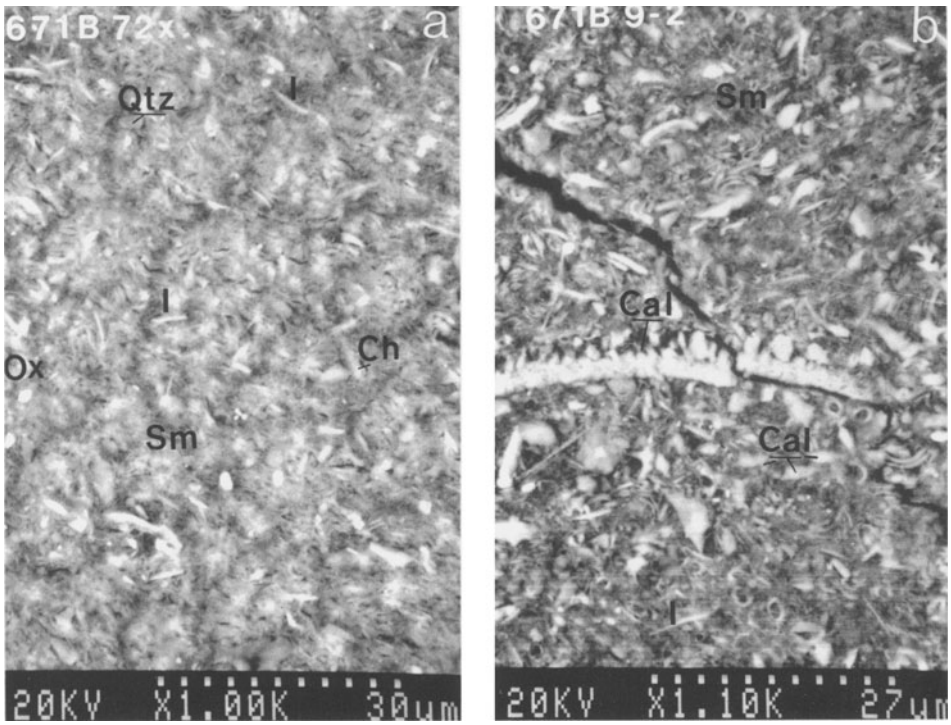


Figure 5. SEM backscattered electron images of sediment thin sections. (a) Deep sample (670 meters) with a weak foliation in the NW–SE direction, and showing quartz, oxides (bright contrast), detrital illite and chlorite in a matrix of smectite. (b) Shallow sample (70 meters) with no foliation, but showing detrital illite and many calcite grains (bright contrast) in a matrix of smectite. Cal = calcite; Sm = random mixed-layer illite/smectite; Ox = FeTi oxides; I = detrital illite; Ch = chlorite; QTZ = quartz.

sample. The peak is asymmetric and less sharp for air-dried and glycerol-treated samples of specimens 671B 61-05, 671B 64-4, 671B 67-05 and 671B 72X, implying the presence of a higher proportion of illite layers in the I/S. A small peak at 10 Å is also present for all air-dried samples, occurring at 10 Å after glycolation, and reflecting the presence of detrital mica or illite at all depths in the sediment column. A 7.2-Å peak due to kaolinite (±chlorite) is present in all air-dried and glycolated samples. These diffraction patterns are consistent with, and representative of, the much larger number of samples analyzed by Capet *et al.* (1990) and Tribble (1990).

SEM and backscattered electron images

Low-magnification images show that the samples consist of a small proportion of large grains that are more than 10 μm in size and that are inferred to be detrital in origin. The grains are surrounded by a fine-grained matrix that appears grey in backscattered images (Figure 5). The large detrital grains in the shallowest samples are predominantly calcareous nannofossils larger than 20–30 μm, and have bright contrast in BSE images (Figure 5b). Such nannofossils are rare or absent in the deepest samples [671B 64-4 (52–54) and 671B 72X (38–40)], presumably because they have been lost by dissolution. Large-scale dissolution of carbonates in Miocene sediments occurred through upward migration of the calcium carbonate compensation depth (CCD) (Clark, 1990). Clasts of feldspar, quartz, titanomagnetite, pyrite, and calcite are visible in these samples. The clay fraction is represented by large grains of mica, kaolinite and chlorite in all samples. The mica grains, which have a muscovite-like composition as shown by EDS analyses, are up to 3 μm in diameter and 0.1 μm thick. SEM resolution does not permit identification of individual matrix mineral grains. However, EDS analyses of this matrix show the presence of major Si and Al with minor Ca, Na, and K, consistent with smectite or I/S. Texture varies in a regular way with depth: in the deepest samples, the large grains have the same bedding-parallel orientation, whereas the shallowest samples have no preferred orientation (Figures 5a, b), suggesting that the sediments are more compact in the deeper samples.

TEM images and STEM chemical data

The majority of material observed using samples with grains dispersed on holey carbon is anhedral, with completely irregular outlines. EDS analyses confirmed that this material is smectite or I/S. The clay particles display the cornflake-like morphology with curved

https://doi.org/10.1346/CCMN.1992.0400108 Published online by Cambridge University Press

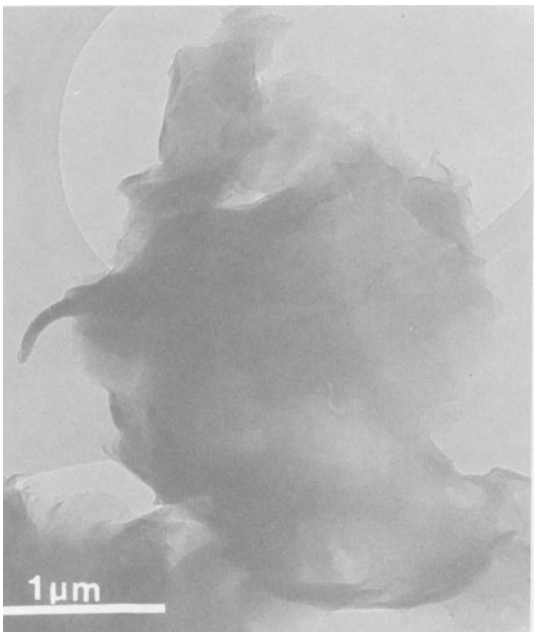


Figure 6. TEM image of a smectite flake in the clay fraction showing the typical "cornflake" texture.

edges that is typical of smectite found in marine sediments (Figure 6) (e.g., Buatier *et al.,* 1989; Clauer *et al.,* 1990). The dominant smectite is accompanied by anhedral grains of quartz, feldspars, and Fe and Ti oxides, as well as large crystals of illite and kaolinite. Large illite (mica) crystals display a mottled contrast and their SAED patterns are well-defined hexanets implying that they are well-defined single crystals. Kaolinite crystals are easily recognized by their hexagonal shape, rapid beam damage to which they are characteristically subjected, and qualitative EDS analyses that showed the presence only of approximately equal amounts of Al and Si.

At relatively low magnification, the texture of the ion-milled samples consists primarily of sparse, anhedral grains of quartz, feldspar, titanomagnetite, and phyllosilicates that are immersed within a matrix consisting largely of clay minerals (Figure 7). The individual anhedral grains are inferred to be detrital on the basis of their shapes, sizes and compositions. Irregular quartz grains are enclosed within anastomosing smectite. All feldspars are end-member K feldspar in composition, suggesting they are authigenic. Detrital feldspars are heterogeneous (e.g., McDowell, 1986). Anhedral crystals of titanomagnetite were observed in many samples. However, in the deepest samples titanomagnetite is rare, but euhedral titanium oxide crystals were observed that have a rhombic cross section, 200–500 Å square. The euhedral morphology and its occurrence only in the deepest samples where titanomagnetite was not detected, suggest that it is authigenic and owes its origin to dissolution of titanomagnetite.

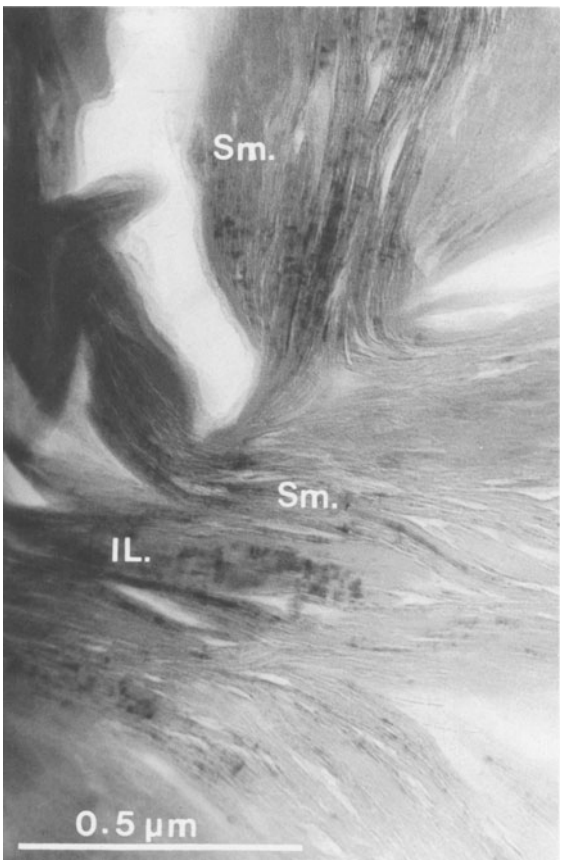


Figure 7. Low magnification TEM image of an ion-milled sample (470 meters). A large detrital illite (mica) grain is embedded in a matrix of smectite. Lenticular spaces within smectite are caused by contraction of the smectite in the vacuum of the electron microscope.

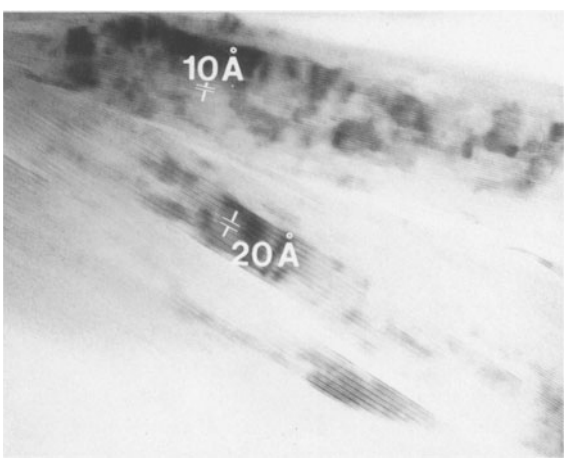


Figure 8. High-resolution lattice-fringe image of two small detrital illite (mica) platelets having typical mottled contrast and showing 10-Å and 20-Å periodicity (2*M* polytype). The grain showing the 10-Å periodicity is not at the correct orientation for detection of two-layer polytypism.

https://doi.org/10.1346/CCMN.1992.0400108 Published online by Cambridge University Press

The large phyllosilicate grains observed both by SEM and at low TEM magnifications, and inferred to be detrital in origin, are enclosed within a matrix of clay minerals with curved layers (Figure 7). They were identified using lattice-fringe images, SAED patterns, and EDS analyses. Chlorite, kaolinite, 2*M* illite/mica, and a 14/10 Å mixed-layer phase were identified (Figures 8–10). 2*M* illite was observed in all specimens. Individual grains are composed of subparallel, defect-free 10-Å layers, and display the characteristic "mottled" contrast commonly observed in micas and attributed to cation diffusion induced by the electron beam (Ahn and Peacor, 1986a; Jiang *et al.*, 1990). SAED patterns and lattice-fringe images show that the micas are well-crystallized two-layer polytypes. Chemical analyses reflect a range of compositions, with Al/Si ratios of approximately 0.7 to 0.8, moderate Fe and Mg contents, and variable K contents. Some formulae in Table 1A have a high octahedral contribution to the negative charge, similar to that of the phengite formulae described by Shau *et al.* (1991). The low K contents are due to alkali ion diffusion induced by the electron beam (van der Pluijm *et al.*, 1988). Because of the problem of alkali diffusion, the structural formulae of illite were normalized to a total of 12 cations in the octahedral and tetrahedral sites, assuming that these clays are dioctahedral [which is the case according to data of Capet *et al.* (1990) regarding 060 peaks from XRD patterns]. Both phengite- or illite-like compositions and 2*M* polytypes are characteristic only of relatively high grades of diagenesis and metamorphism. These data, their occurrence even in the shallowest samples, their large sizes and irregular shapes all show that the micas are detrital in origin. The chlorite grains that were occasionally observed in all specimens occur as packets of well-defined 14-Å layers as seen in the lattice-fringe images. They vary in Mg/Fe ratio, as expected for such detrital material, some being Mg-rich and some Fe-rich. Chemical data determined from EDS analysis with normalization to 11 oxygens are presented in Table 1B. Rare, coarse grains with irregularly interstratified 10- and 14-Å layers were also observed in all samples. According to lattice-fringe images, SAED patterns, and EDS analyses (Figure 10 and Table 1), they are irregularly interstratified illite/chlorite. A typical composition, calculated on the basis of 25 O atoms (14 O atoms for the chlorite layer and 11 for the illite layer), is $K_{0.8}[Mg_{3.1}Fe_{2.6}Al_{2.4}][Si_{6.5}Al_{1.5}]$ corresponding to approximately 50% illite and 50% chlorite. Mixed-layering of dioctahedral and trioctahedral phyllosilicates has never been reported on the basis of XRD analysis of sediments. However, using TEM lattice-fringe images, mixed-layer illite/chlorite has been observed as a product of plagioclase alteration (Page and Wenk, 1979), and in shales and slates (Kniper, 1981; Lee *et*

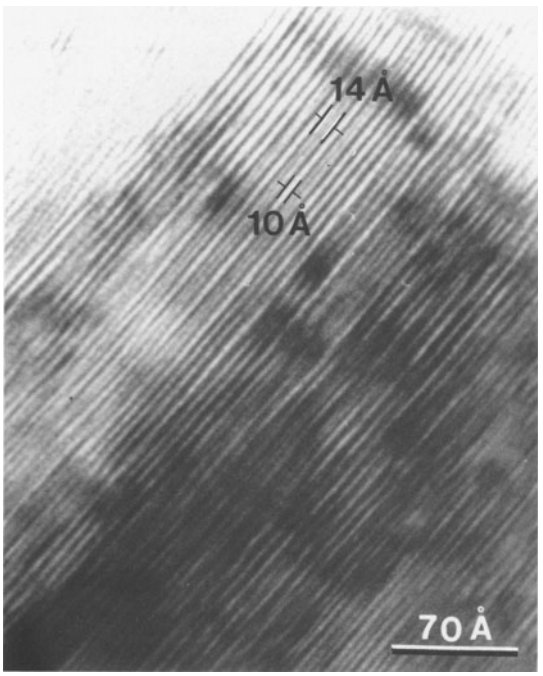


Figure 10. High-resolution lattice-fringe image of a large detrital grain showing interstratified 10-Å (illite) and 14-Å (chlorite) layers.

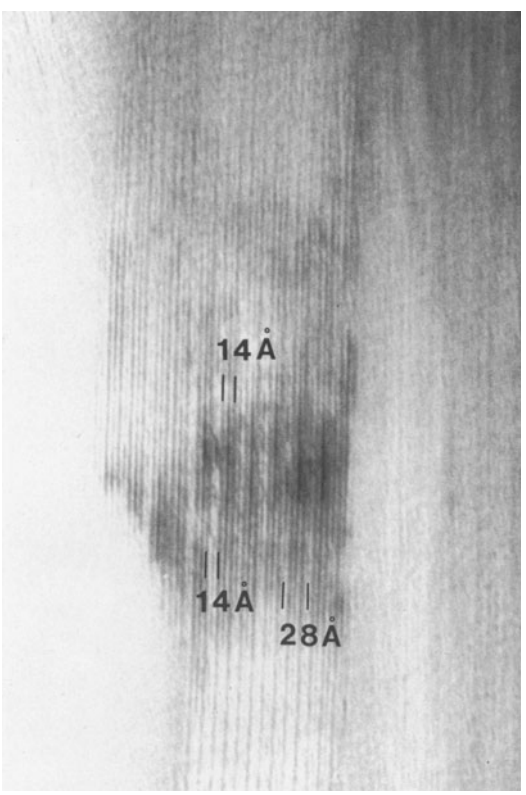


Figure 9. High-resolution lattice-fringe image of a detrital chlorite showing two-layer polytype (28 Å).

https://doi.org/10.1346/CCMN.1992.0400108 Published online by Cambridge University Press

Table 1A. AEM analyses obtained with a 1000 Å-square window on several samples. Data represent detrital micas. The analyses were normalized for 12 cations in tetrahedral and octahedral sites.

		2M detrital mica (illite and phengite)						
	Oxide (wt. %)	72X(1d)*	51-2(1d)	64-4(1d)	51-2(2d)	51-2(3d)	51-2(4d)	64-4(2d)
	Na_2O	0.52	1.27	0.95	0.61	0.87	0.53	0.74
	MgO	2.96	2.33	3.77	2.11	2.23	3.03	1.10
	Al_2O_3	23.71	33.66	27.80	31.86	36.13	33.89	30.62
	SiO_2	50.95	48.69	52.00	53.09	48.97	49.66	53.46
	K_2O	9.36	8.20	7.16	5.57	5.05	5.14	6.60
	CaO	0.34	0.00	0.22	0.21	0.65	0.84	0.15
	TiO_2	0.27	0.00	0.61	0.00	0.00	0.00	0.00
	MnO	0.00	0.00	0.00	0.00	0.00	0.00	0.00
	Fe_2O_3	6.88	0.84	2.50	1.55	1.76	2.74	2.33
	Total	95.00	95.00	95.00	95.00	95.00	95.00	95.00
	Cation	No. of cations						
Tetrahedral site	Si	6.87	6.31	6.60	6.70	6.10	6.18	6.89
	AlIV	1.13	1.69	1.40	1.30	1.90	1.82	1.11
Octahedral site	AlVI	2.61	3.45	2.73	3.65	3.40	3.15	4.64
	Fe^{3+}	0.77	0.09	0.26	0.16	0.18	0.26	0.25
	Mg	0.59	0.46	0.71	0.40	0.42	0.20	0.21
	Mn	0	0.00	0.00	0.00	0.00	0.00	0.00
	Ti	0.03	0.00	0.26	0.00	0.00	0.00	0.00
Interlayer site	Na	0.14	0.32	0.23	0.15	0.21	0.13	0.19
	K	1.61	1.35	1.16	0.90	0.80	0.82	1.08
	Ca	0.05	0.00	0.03	0.03	0.00	0.00	0.02
	Σ cations	13.8	13.67	13.42	13.08	13.01	12.95	13.27

* The number in parentheses indicates the analysis number.

Table 1B. AEM analyses obtained with a 1000 Å-square window on several samples. They represent illite-chlorite mixed layers and chlorite analyses. The analyses were normalized to 25 oxygens for the analyses of illite/chlorite and 14 oxygens for the chlorite analyses.

		Detrital illite/chlorite				Detrital chlorite		
	Oxide (wt. %)	64-4(3d)*	54-4(1d)	64-4(4d)	64-4(5d)	51-2(5d)	64-4(6d)	51-2(6d)
	Na_2O	1.82	0.67	2.36	1.75	0.00	0.00	0.00
	MgO	8.62	7.44	6.45	5.56	20.15	17.61	16.33
	Al_2O_3	17.47	14.34	20.48	22.65	15.76	24.58	24.29
	SiO_2	37.36	38.54	33.59	41.47	36.17	29.34	32.58
	K_2O	2.00	7.55	1.46	3.08	0.00	0.00	0.00
	CaO	0.16	0.32	0.23	0.18	0.25	0.00	0.00
	TiO_2	0.00	1.99	0.00	0.00	0.00	0.00	0.00
	MnO	0.45	0.45	0.28	0.15	0.92	0.00	0.00
	Fe_2O_3	20.11	16.71	23.16	13.17	14.74	16.47	14.8
	Total	88.00	88.00	88.00	88.00	88.00	88.00	88.00
	Cation	No. of cations						
Tetrahedral site	Si	6.72	7.05	6.17	7.09	3.53	2.89	3.15
	AlIV	1.28	0.95	1.83	0.91	0.47	1.11	0.85
Octahedral site	AlVI	2.43	2.14	2.61	3.65	1.34	1.74	1.92
	Fe	3.03	2.55	3.56	1.88	1.20	1.36	1.20
	Mg	2.31	2.03	1.77	1.41	2.93	2.58	2.35
	Mn	0.07	0.07	0.04	0.02	0.08	0.00	0.00
	Ti	0.00	0.27	0.00	0.00	0.00	0.00	0.00
Interlayer site	Na	0.64	0.24	0.84	0.58	0.00	0.00	0.00
	K	0.46	1.76	0.34	0.67	0.00	0.00	0.00
	Ca	0.03	0.06	0.04	0.03	0.03	0.00	0.00
	Σ cations	16.97	17.13	17.20	16.26	9.57	9.68	9.47

* The number in parentheses indicates the analysis number.

https://doi.org/10.1346/CCMN.1992.0400108 Published online by Cambridge University Press

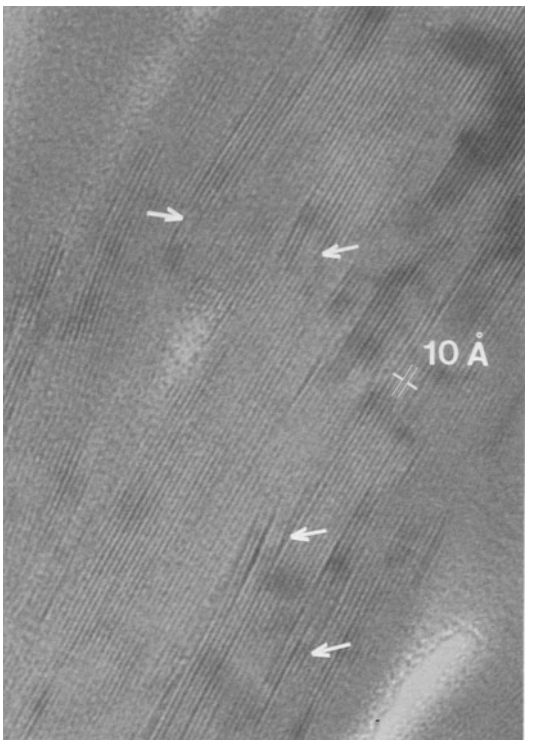


Figure 11. High-resolution lattice-fringe image of smectite containing a small proportion of interlayered illite (<20%) in sample 51-2 (470 meters). Layers are typically curved and discontinuous, with dislocations (layer terminations) indicated by arrows. They have a 10-Å periodicity inferred to result from collapse of 14-Å layers in high-vacuum environment.

al., 1984; Lee and Peacor, 1985). The large size and irregular shapes of these grains and their enclosure within the continuous clay matrix are consistent with a detrital origin.

The matrix consists principally of smectite (with some illite layers) that occurs as discontinuous anastomosing layers enclosing the relatively large detrital grains. While difficult to obtain because of rapid beam damage, lattice-fringe images displayed 10-Å curved layers (resulting from collapse of 14-Å layers in the high vacuum environment) with a high density of edge dislocation-like layer terminations (Figure 11). The diffraction patterns display weak *hkl* reflections that occur as continuous streaks reflecting a $1M_d$ structure, i.e., a completely random stacking of layers. This smectite is potassium-rich (Table 2). Some K could reside in illite interlayers within smectite as implied by some TEM images (obtained under overfocus conditions) with strongly contrasting 10-Å fringes. The XRD data, however, imply that the proportion of such interlayers is very small, and that they would account for only a small fraction of the analyzed K. Most of the K must therefore occur in smectite interlayers. The tetrahedral charge is approximately 0.4 to 0.6. Smectite ordinarily has cations such as Ca and Na in interlayer sites. The presence of significant K is very unusual. Indeed, some clay mineralogists believe that the presence of K may cause collapse of the interlayers and formation of illite, which if true implies that high K contents are not likely

Table 2. AEM analyses obtained with a 1000 Å-square window on the smectite (±I/S) from the shallow samples. The analyses were normalized for 12 cations in tetrahedral and octahedral sites.

Oxide (wt. %)		54-4(1)*	54-4(2)	54-4(3)	51-2(3)	51-2(4)	51-2(5)	51-2(6)	51-2(7)	51-2(8)	51-2(9)	51-2(10)	51-2(11)	51-2(12)
Na_2O		0.72	0.00	0.63	2.04	2.05	0.76	1.07	1.17	0.85	1.26	1.66	1.28	0.99
MgO		2.28	1.28	3.03	5.27	4.36	4.17	4.31	3.93	3.34	4.43	4.14	4.24	3.78
Al_2O_3		24.83	16.45	15.82	16.69	18.38	18.81	17.38	18.82	19.71	18.70	19.16	17.66	16.35
SiO_2		52.07	49.69	52.70	55.67	52.33	56.36	55.79	55.24	57.91	54.40	53.92	56.33	58.47
K_2O		3.27	2.22	1.21	0.64	1.75	0.86	0.89	1.51	0.63	2.24	1.17	0.68	0.62
CaO		0.24	0.96	0.30	0.47	0.43	0.50	0.59	0.51	0.41	0.68	0.57	0.70	0.32
TiO_2		0.00	0.58	0.44	0.00	0.00	0.30	0.00	0.00	0.00	0.00	0.50	0.31	0.19
MnO		0.17	1.10	0.56	0.34	0.18	0.20	0.20	0.25	0.16	0.18	0.00	0.19	0.16
Fe_2O_3		4.40	15.73	13.31	6.87	8.52	6.03	7.77	6.56	4.98	6.11	6.89	6.60	7.12
Total		88.00	88.00	88.00	88.00	88.00	88.00	88.00	88.00	88.00	88.00	88.00	88.00	88.00
	Cation	No. of cations												
Tetrahedral site	Si	7.08	7.12	7.36	7.53	7.23	7.57	7.56	7.51	7.73	7.44	7.37	7.64	7.88
	AlIV	0.91	0.88	0.64	0.46	0.77	0.43	0.44	0.49	0.27	0.55	0.63	0.36	0.12
Octahedral site	AlVI	3.07	1.90	1.99	2.20	2.22	2.55	2.34	2.53	2.86	2.57	3.08	2.47	2.48
	Fe	0.45	1.70	1.40	0.70	0.88	0.61	0.79	0.67	0.50	0.63	0.71	0.67	0.72
	Mg	0.46	0.27	0.63	1.06	0.90	0.83	0.87	0.79	0.67	0.90	0.84	0.86	0.76
	Mn	0.02	0.13	0.07	0.04	0.02	0.02	0.02	0.03	0.02	0.02	0.00	0.02	0.02
	Ti	0.00	0.06	0.04	0.00	0.00	0.03	0.00	0.00	0.00	0.00	0.05	0.03	0.02
Interlayer site	K	0.57	0.41	0.22	0.11	0.31	0.15	0.15	0.26	0.11	0.39	0.20	0.12	0.11
	Ca	0.04	0.15	0.04	0.07	0.06	0.07	0.08	0.08	0.06	0.10	0.08	0.10	0.05
	Na	0.19	0.00	0.17	0.54	0.55	0.20	0.28	0.31	0.22	0.33	0.44	0.03	0.26
Σ cations		12.8	12.56	12.43	12.72	12.92	12.42	12.51	12.65	12.39	12.82	12.72	12.25	12.42

* The number in parentheses indicates the analysis number.

https://doi.org/10.1346/CCMN.1992.0400108 Published online by Cambridge University Press

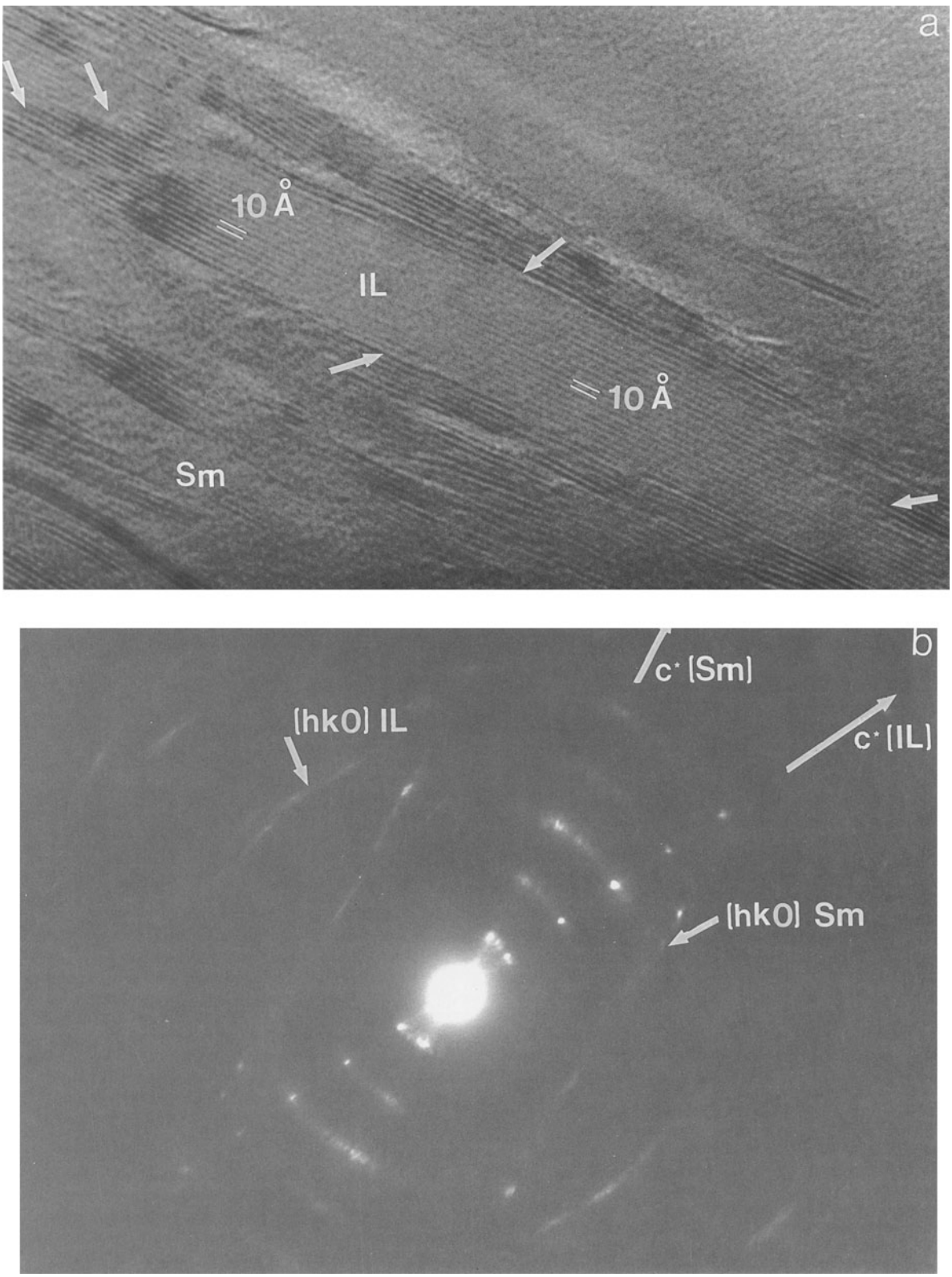


Figure 12. (a) High-resolution lattice-fringe image of a neoformed crystallite of $1M_d$ illite in a matrix of random mixed-layer illite/smectite from a deep sample below the décollement zone (sample 72X), arrow indicates the crystal boundaries.

https://doi.org/10.1346/CCMN.1992.0400108 Published online by Cambridge University Press

in true smectite. Nonetheless, the analytical data are definitive. High proportions of K in interlayer sites of smectite from shallow sediments of the Gulf Coast were also reported recently by Freed and Peacor (in press), who inferred that it was the result of the earliest stage of the smectite-illite transition; i.e., K-exchange in the smectite interlayers.

Tribble (1990) proposed that smectite is at least in part an authigenic phase that was derived by alteration of volcanic glass. Because of the significance of such a process, we searched carefully for such glass using STEM techniques. No volcanic glass, however, was detected. It could have been completely altered in the deepest samples, but its absence in the shallowest sample suggests that glass was present only in the ash layers. These results must be interpreted with caution, as the glass alteration process could have been complete, even in the shallow samples.

All samples have dominant matrix smectite and subsidiary detrital dioctahedral mica, each with nearly identical characteristics. The two deepest samples (671B 64-4 and 671B 72X), however, contained a phase of very different appearance, consisting of small crystallites embedded in the smectite matrix. These crystallites display the typical mottled contrast of dioctahedral micas described by Ahn and Peacor (1986a). At high magnification, they consist of straight lattice fringes with d = 10 Å. The grain boundaries at the ends of the crystallites are well defined with layer terminations displaying steps (Figure 12). Such features are typical of illite that has crystallized directly from solution (Yau *et al.*, 1986, 1987). Because the crystallites are so small, SAED patterns included some surrounding smectite (Figure 12). However, they have sharp (00*l*) spots corresponding to d(001) = 10 Å superimposed on the diffuse (00*l*) reflections typical of smectite. Such sharp reflections occur only in SAED patterns of the crystallites and are therefore ascribed to them. Reflections other than 001 were also observed in some SAED patterns. Such reflections characterize the stacking sequence. In these cases, the reflections were diffuse with streaks parallel to c*, characteristic of the $1M_d$ polytype of illite. The SAED pattern of such crystallites never had the sharp non-00*l* reflections that are typical of detrital illite in all samples from throughout the section. In addition, the crystallites became beam-damaged easily, in contrast with detrital micas, but characteristic of 2:1 phyllosilicates formed through early diagenesis in low-grade rocks (Lee *et al.*, 1984). Chemical analyses of the small crystals were difficult to obtain because their size is at the limit of STEM/EDS resolution and they are rapidly damaged by the electron beam, with resultant diffusion of K. Chemical analyses were, however, obtained of an area 1000-Å square that contained smectite plus a high proportion of crystallites. The resultant compositions, normalized to the formula of a dioctahedral 2:1 phyllosilicate, have approximately 0.5 K atoms per formula unit in Table 3 with a maximum value of 0.9 K. The lower K values probably reflect K diffusion during analysis; most importantly, however, they have high Al contents in tetrahedral sites, with Al/Si = 0.10 to 0.16. Such compositions are markedly different from those of detrital micas but are typical of mixed-layer I/S or illite derived early in the process of transition from smectite. Figure 13 shows the variation of the composition of smectite with depth. The smectite that contains $1M_d$ illite crystallites (most abundant in sample 72X) contains higher K and Al and less Mg than smectite from the shallower samples (e.g., sample 51-2).

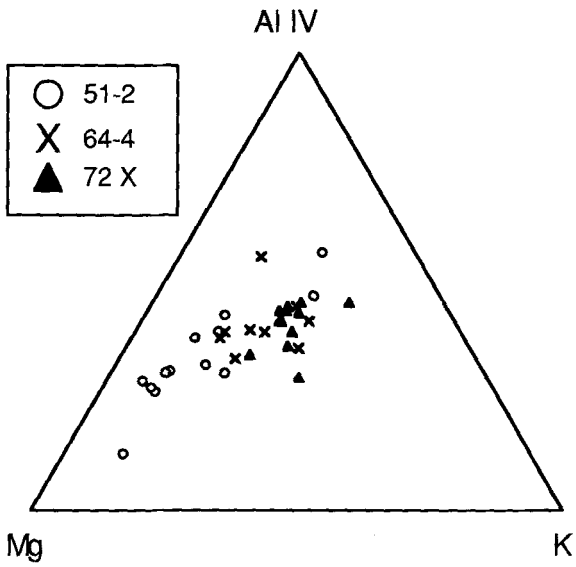


Figure 13. Plot of compositional data for matrix smectite, random mixed-layer I/S, and mixture of neoformed illite and matrix of random I/S. The values plotted are the relative numbers of cations in the structural formulae of a dioctahedral 2:1 phyllosilicate, normalized to 8 tetrahedral cations. There is a clear trend as a function of depth, with the deeper samples being enriched in Al and K and poor in Mg.

DISCUSSION

TEM and AEM data show that sediments in the Barbados accretionary wedge consist primarily of smectite (with some illite layers), a small amount of

←
The ends of the crystal display steps typical of hydrothermally-grown illite. (b) Corresponding SAED pattern with superimposed reflections from illite (IL) and random mixed-layer I/S. The diffuse, ill-defined non-00*l* reflections of illite are typical of $1M_d$ illite (or I/S R = 1).

https://doi.org/10.1346/CCMN.1992.0400108 Published online by Cambridge University Press

Table 3. AEM analyses obtained with a 1000 Å-square window on the smectite + neoformed illite from the deepest samples 64-4 and 72X. The analyses were normalized for 12 cations in tetrahedral and octahedral sites.

	Oxide (wt. %)	64-4(1)*	64-4(2)	64-4(3)	64-4(4)	64-4(5)	64-4(6)	64-4(7)	64-4(8)	64-4(9)
	Na_2O	2.64	1.87	1.73	2.05	1.41	1.70	1.28	1.62	1.78
	MgO	3.19	2.54	3.82	3.43	2.87	2.34	2.88	2.84	3.07
	Al_2O_3	13.76	20.85	19.34	19.29	19.31	21.53	20.55	20.15	17.92
	SiO_2	51.27	51.13	54.13	54.09	53.76	51.82	53.11	50.31	52.24
	K_2O	1.43	2.83	2.12	1.46	1.83	1.40	3.36	3.81	2.38
	CaO	0.66	0.00	0.47	0.33	0.22	0.36	0.00	0.22	0.34
	TiO_2	0.00	0.59	0.00	0.00	0.00	0.00	0.00	0.00	0.00
	MnO	0.26	0.00	0.00	0.00	0.00	0.00	0.00	0.00	0.00
	Fe_2O_3	4.78	8.19	6.40	7.35	8.61	8.85	6.81	9.05	10.27
	Total	88.00	88.00	88.00	88.00	88.00	88.00	88.00	88.00	88.00
	Cation	No. of cations								
Tetrahedral site	Si	7.39	7.16	7.43	7.42	7.39	7.12	7.35	7.09	7.32
	AlIV	0.61	0.84	0.57	0.58	0.60	0.88	0.65	0.91	0.68
Octahedral site	AlVI	1.73	2.60	2.56	2.54	2.53	2.60	2.70	3.35	2.27
	Fe	1.60	0.86	0.66	0.76	0.89	0.92	0.71	0.96	1.08
	Mg	0.69	0.53	0.78	0.70	0.59	0.47	0.59	0.60	0.64
	Mn	0.03	0.00	0.00	0.00	0.00	0.00	0.00	0.00	0.00
	Ti	0.00	0.06	0.00	0.00	0.00	0.00	0.00	0.00	0.00
Interlayer site	K	0.26	0.51	0.37	0.25	0.32	0.24	0.59	0.68	0.42
	Ca	0.10	0.00	0.07	0.05	0.03	0.05	0.00	0.03	0.05
	Na	0.74	0.51	0.46	0.54	0.38	0.57	0.20	0.44	0.48
	Σ cations	13.1	13.02	12.9	12.84	12.73	12.86	12.79	13.15	12.95

* The number in parentheses indicates the analysis number.

large detrital grains of quartz, feldspar, titanomagnetite, and other phyllosilicates. The most important detrital phyllosilicates are 2*M* illite, phengite and kaolinite, but chlorite and mixed-layer illite/chlorite were also observed. All such detrital grains are relatively large (1–10 μm), occur at all depths for which specimens were studied, and are entirely enclosed within a matrix of smectite.

The smectite matrix is very homogeneous in composition and is marked by an unusually high content of interlayer K. The deepest-studied samples, however, contain packets of straight, well-defined 10-Å layers for which EDS data, polytypism, propensity for beam damage, and shape indicate an authigenic origin. XRD data for these samples are consistent with random mixed-layer I/S with about 50% illite layers. By contrast, XRD data for shallower samples indicate the presence of random I/S with less than 20% illite layers, and the packets of authigenic illite are not observed.

The origin of the Barbados sediments

In order to ascertain the origin of the clay minerals in the sediments, the environment that prevailed during their formation must be defined. During the Eocene, hemipelagic sedimentation occurred below the carbonate compensation depth (CCD). From late Eocene to middle Oligocene time, terrigenous material from South America was dominant. From the late Oligocene, the accretionary wedge was active and arc volcanoes produced volcanic ash that was deposited with the terrigenous fractions. Capet *et al.* (1990) suggested that most of the clay was detrital in origin and that it did not occur in volcanic ash layers. They inferred that smectite and kaolinite were derived from soils of the Antilles arc islands where alteration was favored by a humid tropical climate. These minerals were detected in the soils of Martinique by Julius and Pons (1972). Capet *et al.* (1990) concluded that illite and chlorite are also detrital and that they were derived from South America and transported from the Orinoco delta by submarine currents (Bouysse *et al.*, 1990). The mineralogical data of this study confirm the detrital origin of kaolinite, 2*M* mica, and chlorite as indicated by the large grain sizes, polytypism, shape, relation to smectite matrix, and compositions. These minerals appear as large crystals with irregular outlines, except for some kaolinite. XRD data show that they collectively make up approximately 20 to 30% of the clay fraction of the sediments. They probably were derived from South America and were transported by wind and ocean currents to their site of deposition.

Hypotheses concerning the origin of the smectite have been discussed in Moore, Mascle *et al.* (1990). As noted above, Capet *et al.* (1990) emphasized that smectite is detrital, having been derived by weathering of volcanogenic soils on volcanic island arcs. However, Tribble (1990) suggested that some of the smectite is derived from *in situ* alteration of volcanic ash in the marine sediment as a diagenetic process. The latter

https://doi.org/10.1346/CCMN.1992.0400108 Published online by Cambridge University Press

Table 3. Continued.

64-4(10)	64-4(11)	72X(1)	72X(2)	72X(3)	72X(4)	72X(5)	72X(6)	72X(7)	72X(8)	72X(9)	72X(10)
1.24	1.29	2.05	2.09	2.00	1.43	0.59	1.34	2.23	1.4	0.52	1.16
2.68	2.97	2.47	2.40	2.57	2.10	3.97	3.09	2.73	2.49	1.69	3.09
17.66	17.66	20.10	22.83	20.57	21.97	20.69	19.92	19.89	19.04	16.66	18.79
52.76	51.36	51.46	50.75	51.68	47.57	47.99	51.06	51.89	51.83	55.01	54.46
2.70	2.68	2.47	2.89	2.57	5.05	4.72	2.75	2.95	2.34	1.95	2.05
0.36	0.34	0.78	0.30	0.25	0.39	0.31	0.64	0.61	1.04	0.94	0.37
0.00	0.00	0.00	0.00	0.00	0.00	0.00	0.53	0.00	0.67	0.00	0.00
0.18	0.12	0.38	0.00	0.27	0.00	0.15	0.26	0.00	0.00	0.00	0.00
10.42	11.58	8.35	6.74	8.08	9.09	9.58	8.41	7.70	9.19	11.23	8.08
88.00	88.00	88.00	88.00	88.00	88.00	88.00	88.00	88.00	88.00	88.00	88.00
					No. of cations						
7.41	7.22	7.25	7.14	7.21	6.85	6.73	7.12	7.30	7.34	7.71	7.49
0.59	0.78	0.75	0.85	0.79	1.15	1.27	0.88	0.70	0.66	0.29	0.51
2.33	2.14	2.58	2.94	2.59	2.58	2.15	2.39	2.60	2.52	2.46	2.54
1.10	1.22	0.88	0.71	0.85	0.99	1.01	0.88	0.82	0.98	1.18	0.84
0.56	0.62	0.52	0.50	0.53	0.45	0.83	0.64	0.57	0.52	0.35	0.63
0.02	0.01	0.05	0.00	0.03	0.00	0.02	0.03	0.00	0.00	0.00	0.00
0.00	0.00	0.00	0.00	0.00	0.00	0.00	0.05	0.00	0.07	0.00	0.00
0.49	0.48	0.44	0.52	0.46	0.93	0.84	0.49	0.53	0.42	0.35	0.36
0.05	0.05	0.12	0.05	0.04	0.06	0.05	0.10	0.09	0.16	0.14	0.05
0.34	0.35	0.54	0.56	0.54	0.51	0.16	0.36	0.61	0.39	0.52	0.31
12.88	12.88	13.1	13.13	13.04	13.5	13.05	12.95	13.23	12.97	13.01	12.72

hypothesis seems to be confirmed by pore water chemical data that are interpreted by Gieskes *et al.* (1990) to be the result of ash alteration. Alteration reactions involving volcanic ash lead to depletion in Mg^{2+} and K^+ and to low $^{87}Sr/^{86}Sr$ ratios in interstitial fluids.

In summary, two origins have been proposed for the smectite: (1) submarine alteration of volcanic ash (Tribble, 1990), and (2) subaerial alteration of arc volcanic rocks (Capet *et al.,* 1990). AEM data obtained in this study show that the smectite is very homogeneous and K-rich, suggesting that exchange with interstitial fluids occurred after its formation (Perry *et al.,* 1976). Smectite could be formed with some illite-mixed layers. However, the XRD data indicate that smectite from the shallowest samples contains less than 20% illite layers, which implies that a significant amount of K is located in the smectite interlayers. No volcanic ash was detected in the samples studied; they seem to be concentrated in the ash layers. This observation favors the hypotheses of subaerial formation. The origin of smectite, however, cannot be definitively determined here and awaits results of stable isotope analyses in progress.

The smectite-to-illite transition

XRD data and TEM observations for both dispersed clay particles and ion-milled samples bear importantly on our understanding of the smectite-to-illite transition, at least in its initial stage. In ion-milled samples that retain original textures, smectite occurs as a more-or-less continuous matrix, for which there are no grain boundaries, *per se.* Lattice-fringe images are typically wavy and anastomosing, with frequent layer terminations. As seen in separates dispersed on carbon-coated grids, the cleaved smectite appears to be flaky particles with curved edges; i.e., with a cornflake-like appearance.

In ion-milled samples, neoformed illite was observed as small crystallites for which lattice-fringe images have straight, defect-free fringes. The crystallite {001} boundaries are contiguous with parallel smectite fringes, but the narrow edges display steps in terminating fringes, typical of illite known to have crystallized from solution. The same morphological features were observed for synthetic muscovite that grew by addition of individual layers following nucleation (Amouric, 1987) and for phyllosilicates crystallized from hydrothermal solutions in Salton Sea sediments (Yau *et al.,* 1987). The 00*l* reflections of SAED patterns are very sharp, and other reflections than 00*l* are present but ill-defined and diffuse parallel to c*, typical of $1M_d$ illite in its initial stage of formation following transition from smectite (Baxter Grubb *et al.,* 1991). XRD data show that the two deepest samples contain random I/S mixed layers with more illite layers that are present in the shallowest sample. All data are therefore independently consistent with the occurrence of illite that represents the initial stages of the smectite-to-illite transition.

The identity of the so-called "illite" is subject to some question, however. All TEM data are consistent with both illite, *sensu strictu,* and mixed-layer I/S. For

https://doi.org/10.1346/CCMN.1992.0400108 Published online by Cambridge University Press

example, Inoue *et al.* (1990) have shown that mixed-layer I/S has characteristics, similar to those of the "illite" of this study, and Freed and Peacor (in press) describe nearly identical results for R = 1 mixed-layer I/S occurring in Gulf Coast pelites. Nevertheless, the data are definitive in showing that such material is at least illite-rich, even though some illite/smectite mixed layers may be present.

The observations of this study demonstrate that the mechanism for the smectite-to-illite transition in sediments of the Barbados accretionary wedge is one of dissolution of smectite and crystallization of illite. Growth is inferred to occur by addition of (001) layers, replacing smectite layers as growth proceeds. This process is identical to that proposed by Ahn and Peacor (1986) for Gulf Coast pelites. We refer to it as the "packet theory" because illite grows as a packet of layers with a continuous matrix of smectite. The neoformed crystallites are first observed in our samples at a depth of only 500 meters; they are most abundant in samples located in and below the décollement zone. This smectite-to-illite transition cannot be the result of diagenesis preceding thrusting of the sediments. Indeed, the early Oligocene section where the transition occurred was initially at only 200 meters below the sea water-sediment interface. This transition is probably a consequence of the thrusting of the sediment following formation of the accretionary wedge.

Many authors have claimed that the smectite-to-illite reaction can be used to infer the temperature of transition in basin sediments undergoing diagenesis (Burst, 1969; Hower *et al.,* 1976; Hoffman and Hower, 1979). However, such a relation requires that both the illite and smectite be stable phases and that true chemical equilibrium be attained. Such conditions occur much more readily at temperatures of the greenschist facies and above, for which there are many geothermometers. Jiang and Peacor (1990) showed that illite (and smectite) is a metastable phase. They and other authors (e.g., Ahn and Peacor, 1989; Freed and Peacor, 1989; Inoue *et al.,* 1990) have noted that the degree of illitization is also influenced by the chemistry of the fluids and the porosity and permeability of the strata (i.e., the water/rock ratio). According to Ahn and Peacor (1986) and Jiang *et al.* (1990), the smectite-to-illite transition involves only metastable phases and is therefore controlled by kinetic factors, only one of which is temperature. Water, as a kind of catalyst, is essential for mediating the dissolution, solute transport, and crystallization that have been demonstrated for the samples of this study. Whitney (1990) studied the effect of water on the smectite-to-illite reaction in hydrothermal experiments and found that the rate and extent of illitization was significantly inhibited in fluid-deficient systems. The rate for the reaction is thus increased in the presence of larger water/rock ratios. According to these relations, the reaction may occur at temperatures well below those typical of the smectite-to-illite reaction in Gulf Coast sediments (~100°C), if there is sufficient water. The effect of fluid/rock ratio on feldspar dissolution and illite formation was studied experimentally by Huang *et al.* (1986) who found that it is an important variable in dissolution of primary phases and precipitation of secondary clay minerals.

Measurements of the physical properties of Barbados sediments showed that the smectite-rich sediments are highly porous (Taylor and Leonard, 1990). Furthermore, chemical anomalies of pore fluids suggest that fluids have migrated laterally through the sediments over long distances (Gieskes *et al.,* 1990). The occurrence of the smectite-to-illite transition in the Barbados sediments at depths of only 500 meters (temperature of only 20°–30°C), and in direct association with the décollement zone where the water/rock ratio is high and fluid circulation is very active, is critical to an understanding of the parameters affecting the transition. This is the first case where the transition has been studied in sediments where illite is presently growing. The direct observation of the transition at very low temperatures is therefore definitive in demonstrating that temperature is only one of several variables affecting the rate of reaction, and that water/rock ratio and pore-fluid chemistry are of equal or greater importance. These results also are consistent with the general thesis that smectite and illite are metastable phases, and that the smectite-to-illite reaction represents an example of application of the Ostwald step rule (metastable smectite tends to react progressively through dissolution and crystallization steps toward equilibrium states) wherein the reaction rate is determined by several interacting variables.

CONCLUSIONS

TEM, AEM and XRD data show that the initial stages of the smectite-to-illite transition are taking place presently in smectite-rich sediments of the Barbados accretionary wedge at a depth of only 500 meters below the sediment-sea water interface. The transition process, referred to as the "packet theory," involves dissolution of smectite and crystallization of illite or mixed-layer I/S as packets of layers forming crystals that grow within a continuous smectite matrix.

The occurrence of illite at a depth of only 500 meters, corresponding to a measured temperature of only 30°C, is inconsistent with the use of the smectite-to-illite transition as a geothermometer. The relations are consistent with the transition being determined by an Ostwald-step-rule relation in which unstable smectite transforms to metastable illite with reaction progress being dependent on several factors, including temperature, pore-fluid chemistry, and water/rock ratio. In the case of sediments of the Barbados accretionary wedge, porous sediments and, especially, enhanced fluid flow in the décollement zone promote the transition.

https://doi.org/10.1346/CCMN.1992.0400108 Published online by Cambridge University Press

ACKNOWLEDGMENTS

We are grateful to Peter Vrolijk and Gérard Blanc for providing the specimen collected during Ocean Drilling Project Leg 110. We thank Xavier Capet, Yen-Hong Shau and Wei-Teh Jiang for their helpful discussions. This work was supported by NSF grants OCE-8911446 to J. R. O'Neil and EAR-8817080 to D. R. Peacor, EAR-87-88276 for the SEM and STEM. M. Buatier thanks the Rotary International Foundation who provided part of her salary. INSU/CNRS, program D. B. T., contribution 384 VRA 719.

REFERENCES

Ahn, J. H. and Peacor, D. R. (1986a) Transmission and analytical electron microscopy of the smectite-to-illite transition: *Clays & Clay Minerals* **34,** 165–179.

Ahn, J. H. and Peacor, D. R. (1986b) Transmission electron microscope data for rectorite: Implication for the origin and structure of "fundamental particles": *Clays & Clay Minerals* **34,** 180–186.

Ahn, J. H. and Peacor, D. R. (1989) Illite/smectite from Gulf coast shales: A reappraisal of transmission electron microscope images: *Clays & Clay Minerals* **37,** 542–546.

Amouric, M. (1987) Growth and deformation defects in phyllosilicates as seen by HRTEM: *Acta Cryst.* **B43,** 57–63.

Baxter Grubb, S. M., Peacor, D. R. and Yiang, W. T. (1991) TEM observations of polytypism in illite: *Clays & Clay Minerals* **5,** 540–550.

Blanc, G., Gieskes, J. M., Vrolijk, P. J., Mascle, A., Moore, C. J., Taylor, E., Alvarez, F., Andrieff, P., Barnes, R., Beck, C., Behrmann, J., Brown, K., Clark, M., Dolan, J., Fisher, A., Hounslow, M., McClellan, P., Moran, K., Ogawa, Y. M., Sakai, T., Schoonmaker, J., Wilkens, R., and Williams, C. (1988) Advection de fluides intersticiels dans les séries sédimentaires du complexe d'accretion de la Barbade (Leg 110 ODP): *Bull. Soc. Geol. France* **8,** 453–460.

Bouysse, P., Westercamp, D., and Andreiff, P. (1990) The lesser Antilles island arc: in J. C. Moore, A. Mascle, *et al., Proc. ODP, Sci. Results* **110,** College Station, Texas (Ocean Drilling Program), 29–44.

Buatier, M., Honnorez, J., and Ehret, G. (1989) Fe-smectite-glauconite transition in hydrothermal green clays from the Galapagos spreading center: *Clays & Clay Minerals* **37,** 532–541.

Burst, J. F. (1969) Diagenesis of Gulf Coast clayey sediments and its possible relation to petroleum migration: *Bull. Amer. Assoc. Petrol. Geol.* **53,** 73–93.

Capet, X., Chamley, H., Beck, C., and Holtzapffel, T. (1990) Clay mineralogy of sites 671 and 672, Barbados Ridge accretionary complex and Atlantic abyssal plain: Paleoenvironmental and diagenetic implications: in J. C. Moore, A. Mascle, *et al., Proc. ODP, Sci. Results* **110,** College Station, Texas (Ocean Drilling Program), 85–96.

Clark, M. W. (1990) Cenozoic calcareous nannofossils from the Lesser Antilles forearc region and biostratigraphic summary of Leg 110: in J. C. Moore, A. Mascle, *et al., Proc. ODP, Sci. Results* **110,** College Station, Texas (Ocean Drilling Program), 129–137.

Clauer, N., O'Neil, J. R., Bonnot-Courtois, C., and Holtzapffel, T. (1990) Morphological, chemical and isotopic evidence for an early diagenetic evolution of detrital smectite in marine sediments: *Clays & Clay Minerals* **38,** 33–46.

Cliff, G. W. and Lorimer, G. W. (1975) The quantitative analysis of thin specimens: *J. Micros.* **103,** 203–207.

Fisher, A. T. and Hounslow, M. W. (1990) Heat flow through the toe of the Barbados accretionary complex: in J. C. Moore, A. Mascle, *et al.. Proc. ODP. Sci. Results* **110.** College Station, Texas (Ocean Drilling Program), 345–360.

Freed, R. L. and Peacor, D. R. (1989) Variability in temperature of the smectite/illite reaction in Gulf coast sediments: *Clay Miner.* **24,** 171–180.

Freed, R. L. and Peacor, D. R. (in press) Diagenesis and the formation of authigenic illite-rich I/S crystals in the Gulf coast shales: TEM study of clay separates: *J. Sed. Petrol.*

Gieskes, J. M., Vrolijk, P., and Blanc, G. (1990) Hydrogeochemistry of the northern Barbados accretionary transect ODP Leg 110: *J. Geophys. Res.* **95,** 8809–8818.

Hoffman, J. and Hower, J. (1979) Clay mineral assemblages as low-grade metamorphic geothermometers: Application to the thrust faulted disturbed belt of Montana, U.S.A.: in *Aspects of Diagenesis,* P. A. Scholle and P. R. Schluger, eds., *Soc. Econ. Paleontol. Mineral. Spec. Publ.* **26,** 55–79.

Hower, J., Eslinger, E. V., Hower, M. E., and Perry, E. A. (1976) Mechanism of burial metamorphism of argillaceous sediments: 1. Mineralogical and chemical evidence: *Geol. Soc. Amer. Bull.* **87,** 725–737.

Huang, W. L., Bishop, A. M., and Brown, R. W. (1986) The effect of the fluid/rock ratio on feldspar dissolution and illite formation under reservoir conditions. *Clay Miner.* **21,** 581–601.

Inoue, A., Watanabe, T., Kohyama, N., and Brusewitz, A. M. (1990) Characterization of illitization of smectite in bentonite beds at Kinnekulle, Sweden: *Clays & Clay Minerals* **38,** 241–249.

Jiang, W. T. and Peacor, D. R. (1990) Transmission and analytical electron microscopic study of mixed-layer illite/smectite formed as an apparent replacement product of diagenetic illite: *Clays & Clay Minerals* **38,** 449–468.

Julius, C. and Pons, J. C. (1972) Contribution a l'étude d'une mangrove dans la région de Vauclin (Martinique): *Bull. Inst. Geol. Bassin Aquitaine* **12,** 181–186.

Kniper, R. J. (1981) The interaction of deformation and metamorphism in slates: *Tectonophysics* **78,** 249–292.

Leclerc-Vanhoeve, M. and Stephan, J. F. (1985) Evolution géodynamique des Caraibes dans le système points chauds: in *Geodynamique des Caraibes* **1,** A. Mascle, ed., Symposium Paris, Technip, Paris, 21–34.

Lee, J. H. and Peacor, D. R. (1985) Ordered 1:1 interstratification of illite and chlorite: A transmission and analytical electron microscopy study: *Clays & Clay Minerals* **33,** 463–467.

Lee, J. H., Peacor, D. R., Lewis, D. D., and Wintsch, R. P. (1984) Chlorite-illite/muscovite interlayered and interstratified crystals: A TEM/STEM study: *Contr. Miner. Petrol.* **88,** 372–385.

Lorimer, G. W. and Cliff, G. (1976) Analytical electron microscopy of minerals: in *Electron Microscopy in Mineralogy,* H. R. Wenk, ed., Springer-Verlag, New York, 506–519.

McDowell, D. S. (1986) Composition and structural state of coexisting feldspars, Salton Sea geothermal state: *Mineral. Mag.* **50,** 75–84.

Moore, J. C. and Mascle, A. *et al.* (1990) *Proc. ODP, Sci. Results* **110,** College Station, Texas (Ocean Drilling Program).

Nadeau, P. H., Wilson, M. J., McHardy, W. J., and Tait, J. M. (1985) The conversion of smectite to illite during diagenesis: Evidence from some illite clays from bentonites and sandstones: *Mineral. Mag.* **49,** 393–400.

Page, R. and Wenk, H. R. (1979) Phyllosilicates alteration of plagioclase studied by transmission electron microscopy: *Geology* **7,** 393–397.

https://doi.org/10.1346/CCMN.1992.0400108 Published online by Cambridge University Press

Perry, E. A., Gieskes, J. M., and Lawrence, J. R. (1976) Mg, Ca O^{18}/O^{16} exchange in the sediment-pore water system, Hole 149 DSDP: *Geochim. Cosmochim. Acta* **40,** 413–423.

Ransom, B. and Helgeson, H. C. (1989) On the correlation of expandability with mineralogy and layering in mixed layering in mixed-layer clays: *Clays & Clay Minerals* **37,** 189–191.

Shau, Y. H., Feather, M. E., Essene, E. J., and Peacor, D. R. (1991) Genesis and solvus relation of submicroscopically intergrown paragonite and phengite in a blueschist from northern California: *Contrib. Miner. and Petrol.* **106,** 367–378.

Taylor, E. and Leonard, J. (1990) Sediment consolidation and permeability at the Barbados forearc: in J. C. Moore, A. Mascle, *et al., Proc. ODP, Sci. Results* **110,** College Station, Texas (Ocean Drilling Program), 289–308.

Tribble, J. (1990) Clay diagenesis in the Barbados accretionary complex: Potential impact on hydrology and subduction dynamics: in J. C. Moore, A. Mascle, *et al., Proc. ODP, Sci. Results* **110,** College Station, Texas (Ocean Drilling Program), 97–110.

van der Pluijm, B. A., Lee, J. H., and Peacor, D. R. (1988) Analytical electron microscopy and the problem of potassium diffusion: *Clays & Clay Minerals* **36,** 498–504.

Whitney, G. (1990) Role of water in the smectite-to-illite reaction: *Clays & Clay Minerals* **38,** 343–350.

Yau, Y. C., Peacor, D. R., Lewis, D. D., and Wintsch, R. P. (1986) Evidence for syntectonic crystallization for the mudstone-to-slate transition at Lehigh Gap, Pennsylvania, U.S.A.: *J. Struct. Geol.* **8,** 767–780.

Yau, Y. C., Peacor, D. R., and McDowell, S. D. (1987) Smectite-to-illite reactions in Salton Sea shales: A transmission and analytical electron microscopy study: *J. Sed. Petrol.* **57,** 335–342.

(Received 15 July 1991; accepted 11 November 1991: Ms. 2119)

https://doi.org/10.1346/CCMN.1992.0400108 Published online by Cambridge University Press